NANO LETTERS

Letter

pubs.acs.org/NanoLett

Experimental Demonstration of Complete 180° Reversal of Magnetization in Isolated Co Nanomagnets on a PMN–PT Substrate with Voltage Generated Strain

Ayan Kumar Biswas,[†] Hasnain Ahmad,[†] Jayasimha Atulasimha,[†,‡] and Supriyo Bandyopadhyay*[,†]

[†]Department of Electrical and Computer Engineering, [‡]Department of Mechanical and Nuclear Engineering, Virginia Commonwealth University, Richmond, Virginia 23284, United States

Supporting Information

ABSTRACT: Rotating the magnetization of a shape anisotropic magnetostrictive nanomagnet with voltage-generated stress/strain dissipates much less energy than most other magnetization rotation schemes, but its application to writing bits in nonvolatile magnetic memory has been hindered by the fundamental inability of stress/strain to rotate magnetization by full 180°. Normally, stress/strain can rotate the magnetization of a shape anisotropic elliptical nanomagnet by only up to 90°, resulting in incomplete magnetization reversal. Recently, we predicted that applying uniaxial stress sequentially along *two different axes* that are not collinear with the major or minor axis of the elliptical nanomagnet will rotate the magnetization by full 180°. Here, we demonstrate this complete 180° rotation in elliptical Co nanomagnets (fabricated on a piezoelectric substrate) at room temperature. The two stresses are generated by sequentially applying voltages to two pairs of shorted electrodes placed on the substrate such that the line joining the centers of the electrodes in one pair intersects the major axis of a nanomagnet at ∼ +30° and the line joining the centers of the electrodes in the other pair intersects at ∼ −30°. A finite element analysis has been performed to determine the stress distribution underneath the nanomagnets when one or both pairs of electrodes are activated, and this has been approximately incorporated into a micromagnetic simulation of magnetization dynamics to confirm that the generated stress can produce the observed magnetization rotations. This result portends an extremely energy-efficient nonvolatile "straintronic" memory technology predicated on writing bits in nanomagnets with electrically generated stress.

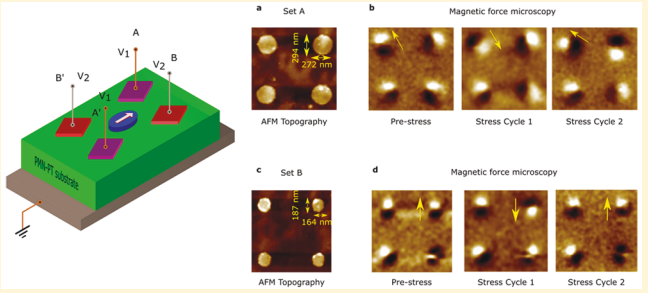

KEYWORDS: *Straintronics, magneto-elastic switching, nanomagnets, piezoelectric*

Nanomagnets are the bedrock of nonvolatile memory. A magnetic random access memory (MRAM) cell is implemented with a magneto-tunneling junction (MTJ) consisting of two nanomagnetic layers, one hard and one soft, separated by a spacer (tunneling) layer. The soft layer is often shaped like an elliptical disc which, if sufficiently thick, has two in-plane stable magnetization directions pointing in opposite directions along the major axis of the ellipse. They encode and store the binary bits 0 and 1. The stored bit is "read" by measuring the resistance of the MTJ which has two discrete values depending on the two magnetization orientations of the soft layer, i.e., for the two bits 0 and 1. The "writing" of bits is accomplished by switching the magnetization of the soft layer between the two antiparallel directions of stable magnetization (180° rotation of the magnetization) with an external agent.

There are many strategies to rotate the magnetization of the soft layer. Popular approaches include passing a spin current through the soft layer to generate a spin transfer torque,[1−6] spin orbit torque[7−10] or domain wall motion.[11,12] Other approaches involve using voltage controlled magnetic anisotropy,[13] magnetoelectric effects,[14−16] magnetoionic effects,[17] and magnetoelastic effects.[18−25] Unfortunately, the generation of a spin current requires passing a charge current through a resistor that dissipates excessive energy, making the spin-current based schemes relatively energy-inefficient.[26,27] The voltage based methods also dissipate energy in charging a capacitor but turn out to be more energy-efficient. One magnetoelastic scheme, the so-called "straintronic" switching, involves rotating the magnetization of a magnetostrictive soft layer with mechanical strain generated by applying a voltage across an underlying piezoelectric layer with a suitable arrangement of electrodes.[28−30] The voltage generates strain in the piezoelectric, which is partially or completely transferred to the elliptical magnetostrictive soft layer, and rotates magnetization by the Villari effect.[19−25] It has been predicted theoretically that large angle (∼90°) rotation in ∼100 nm feature sized nanomagnets made of highly magnetostrictive materials (Terfenol-D, FeGa) will dissipate only ∼1 aJ of energy to occur in ∼1 ns.[31−33]

Received: February 1, 2017
Revised: May 22, 2017
Published: May 26, 2017

DOI: 10.1021/acs.nanolett.7b00439
Nano Lett. 2017, 17, 3478−3484

Recent experiments[34−36] confirm that the energy dissipated to switch a nanomagnet in this fashion will be on the order of 1 aJ in properly scaled structures.

Despite the excellent energy efficiency, straintronic switching is not used for writing bits in MRAMs. What has prevented its use is that strain can normally rotate the magnetization of an elliptical nanomagnet by only up to 90° from either stable orientation along the major axis, placing the final magnetization state along the unstable minor (magnetically hard) axis. Upon strain withdrawal, the magnetization will return to one of the two stable orientations along the major axis, but not necessarily the desired orientation. It has *equal probability* of reaching either orientation. This allows for writing of bits with only 50% success probability, which, of course, is unacceptable. Recently, we proposed a practical approach to increasing the success probability to well over 99.9999% at room temperature in the presence of thermal noise.[37] The trick is to apply uniaxial stresses sequentially in two different directions, noncollinear with the major or minor axis, by activating in succession two pairs of electrodes delineated on the piezoelectric's surface. The two members of each pair are electrically shorted with each other, and either pair is activated by applying a voltage between it and the grounded bottom of the piezoelectric substrate. The electrodes are arranged such that the line joining the centers of the members of one pair subtends an angle of +30°, and the line joining the members of the other pair subtends an angle of −30°, with one direction along the ellipse's major axis. Sequential stressing implemented by sequentially applying voltages to the two electrode pairs rotates the magnetization vector in two steps. In the first step, the magnetization rotates from the initial stable orientation along the major axis by an acute angle. In the second step, the magnetization rotates by an additional angle, bringing it closer to the other stable direction, and finally when the stresses are withdrawn, the magnetization settles into the other stable direction, completing a 180° rotation.[37]

There are other proposed methods of implementing 180° rotation with strain, but they either require very precise timing of the stress cycle which is nearly impossible in the presence of thermal noise at room temperature,[38,39] or special material properties.[40] In contrast, the two-step method does not call for extreme precision, is practical and error-resilient, and works with any magnetostrictive material, whether crystalline, polycrystalline, or amorphous.

Figure 1 shows a cartoon of the 180° rotation scheme. A single elliptical Co nanomagnet is delineated on the surface of a poled piezoelectric substrate. Two pairs of electrodes are placed on the substrate's surface such that the line joining the centers of the electrodes in the first pair AA′ makes an angle of +30° with one direction along the major axis of the nanomagnet and the line joining the centers of the electrodes in the second pair BB′ makes an angle of −30° (or equivalently +330°) with the same direction. The bottom of the substrate is grounded. The direction of substrate poling is such that, when a positive voltage V_1 (= V) is applied between the electrically shorted first pair AA′ and ground, the nanomagnets are elongated along the line $X_{AA'}$ joining the electrode pair and are contracted along the line $Y_{AA'}$ in the perpendicular direction (see the right vertical panel of Figure 1b).[28] A tensile strain ϵ_{xx} is generated in the nanomagnet along $X_{AA'}$, and a compressive strain ϵ_{yy} is generated along the line $Y_{AA'}$. An effective tensile strain $(\epsilon_{xx} - \epsilon_{yy})$ is generated along $X_{AA'}$. Since Co has a negative magnetostriction coefficient, the nanomagnet's magnetization

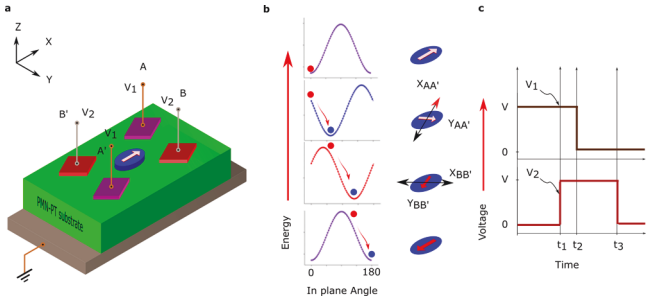

Figure 1. Strain-induced complete magnetization reversal scheme. (a) An elliptical Co nanomagnet is fabricated at the intersection of the lines joining the centers of two pairs of electrodes AA′ and BB′ delineated on a poled piezoelectric $Pb(Mg_{1/3}Nb_{2/3})O_3$−$PbTiO_3$ (PMN−PT) substrate whose bottom is grounded. The substrate is poled with an electric field in the z-direction. The lines AA′ and BB′ subtend angles of +30° and −30°, respectively, with the major axis of the elliptical nanomagnet. (b) The potential energy of the nanomagnet as a function of the angle that its magnetization subtends with the major axis is shown in the left panel for four stressing scenarios—neither electrode pair is activated with a voltage, only AA′ is activated, only BB′ is activated, and both are deactivated. The red dot denotes the initial orientation of the magnetization and the blue dot the final orientation in any stressing scenario. The final orientation always conforms to an energy minimum. The right panel shows the magnetization orientations corresponding to the minima in the corresponding potential energy profiles in the left panel; i.e., they are the stable orientations in the four different stressing scenarios. (c) The timing diagram of the voltage pulses at the two electrode pairs. Figures are not drawn to scale.

rotates through an acute angle from the initial orientation shown in Figure 1a and aligns along the direction perpendicular to the strain axis, i.e. along $Y_{AA'}$ (see the right panel of Figure 1b). The potential energy profile in the plane of the magnet, drawn as a function of the angle that the in-plane component of the magnetization subtends with the initial direction along the major axis, is shown in the left panel of Figure 1b for the four different stressing scenarios: no electrode is activated with a voltage, only AA′ is activated, only BB′ is activated, and both electrodes are deactivated. Note that activating AA′ places the magnetization at an acute angle from the initial orientation. Next, a positive voltage V_2 (= V_1 = V) is applied between the electrically shorted second pair BB′ and ground at time t_1 while turning off the voltage (V_1) at pair AA′ after a time t_2 ($t_2 \geq t_1$). This will again generate an effective tensile strain $(\epsilon_{xx} - \epsilon_{yy})$ along the line $X_{BB'}$, and the magnetization rotates further and aligns in the direction $Y_{BB'}$ perpendicular to that of the new strain axis along BB′. The new energy profile in the plane of the magnet (third row of Figure 1b) shows that the magnetization has rotated (clockwise or counterclockwise) through an obtuse angle from the initial orientation shown in the first row. Finally, the voltage (V_2) is turned off at time t_3 ($t_3 > t_1, t_2$), whereupon the bistable energy profile is restored and the magnetization settles down in the direction that is *opposite* to the initial direction since it cannot transcend the energy barrier that separates the last orientation from the initial one.[37] This completes a 180° rotation. The same rotation would occur if we reversed the sequence of stress application from (AA′, BB′) to (BB′, AA′), except that in one case, the rotation will take place clockwise and in the other case counterclockwise. Note that, if we activated only one pair of electrodes—either AA′ or BB′—and not the other, then the magnetization will have rotated through an acute angle from the initial orientation and finally

DOI: 10.1021/acs.nanolett.7b00439
Nano Lett. 2017, 17, 3478−3484

returned to the initial orientation after electrode deactivation, resulting in 0° rotation.

Note also that there are no restrictions on the time durations t_1, t_2, and t_3, except that they must exceed the times it takes for the magnetization to rotate between the intermediate states. Since the latter are uncertain in the presence of thermal noise, we merely need to ensure that t_1, t_2, and t_3 are larger than the statistically largest possible rotational durations. Thus, there is no critical precision demand on t_1, t_2, or t_3, which makes the scheme practical.

To demonstrate this scheme experimentally, we have fabricated the structure of Figure 1a, except that we made large area contact pads and placed several nanomagnets between them instead of a single nanomagnet. This was done to make the lithography tractable without compromising the demonstration. The nanomagnets are arranged with their major axes mutually parallel (within lithographic tolerance), such that the lines AA′ and BB′ joining the electrode pairs subtend angles of $\sim \pm 30°$ with one direction of the major axis. All nanomagnets are initially magnetized along one direction of the major axes with a global magnetic field of 0.2 T. The magnetization states of the nanomagnets before and after the application of voltage generated stresses are determined by magnetic force microscopy (MFM) using a low moment tip.

Figure 2a shows AFM images of four nanomagnets which are ~700 nm apart from each other (center-to-center distance between nearest neighbors). The large intermagnet distance ensures that dipole interactions between nanomagnets are negligible, and each nanomagnet can be viewed as "isolated" from its neighbors. The major and minor axes of the nanomagnets are measured from the AFM image to be 198 and 183 nm, respectively. The nominal nanomagnet thickness is 8 nm, as determined during deposition, but we will assume it to be 7 nm to allow for 1 nm of surface oxidation. With these dimensions, the in-plane shape anisotropy energy barrier in a nanomagnet is calculated to be 4.191 eV. It is not so large that stress cannot overcome it in the manner of Figure 1b and make the magnetization switch and yet not so small that the magnetized MFM tip could alter the magnetization during scanning. The energy barrier is also large enough to guarantee excellent thermal stability. Figure 2b shows the MFM images of these nanomagnets after magnetization by the global magnetic field and before application of any stress. It is evident from Figure 2b that the magnetic field aligns all but one nanomagnet's magnetization more or less along the field. They are not *exactly* along the field since the magnetization will seek out the closest easy axis, which may not be exactly along the major axis because the magnet shapes are not perfectly elliptical. However, the outlier nanomagnet in the top left corner is magnetized almost opposite to the magnetic field. Its failure to align its magnetization along or close to the magnetic field can be ascribed to a variety of effects but most likely is caused by pinning of the magnetization in the direction almost opposite to the applied field. Note that all nanomagnets exhibit near single domain characteristics with distinct N−S poles.

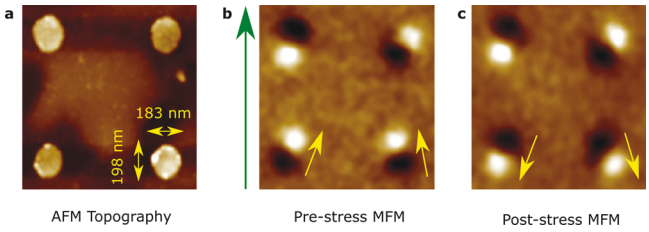

Figure 2. Atomic force micrographs (AFM) and magnetic force micrographs (MFM) of four nominally identical elliptical Co nanomagnets delineated on a PMN−PT substrate showing how their magnetizations evolve with stress. (a) AFM image showing the topography of the nominally elliptical nanomagnets. (b) The nanomagnets are magnetized with a high magnetic field (~0.2 T) in the direction of the green arrow (approximately parallel to the major axes of the ellipses) prior to applying stress. After field withdrawal, each nanomagnet's magnetization rotates to the nearest easy axis (energy minimum) which may not be exactly along the major axis of the ellipse because the magnets' shapes are not perfectly elliptical. The top left nanomagnet's magnetization was unaffected by the field; it is pinned in a stable single domain state that is magnetized nearly antiparallel to the applied field. The pinning can be caused by lithographic imperfections, zagged edges (as evident from AFM image in panel a), or defects. (c) MFM image of poststress magnetization states (after electrode pairs AA′ and BB′ had been sequentially activated). The pinned nanomagnet and the other one in the top row have not rotated under sequential stress, while the two nanomagnets in the bottom row have rotated through 180°. The yellow arrows show the magnetization orientations of the two responsive nanomagnets in the bottom row pre- and poststress.

Next, one of the electrode pairs (AA′) is activated by imposing a voltage of 300 V between it and the grounded bottom of the substrate. This results in an average vertical electric field of 0.6 MV/m along the substrate's thickness underneath the electrodes which generates a highly localized out-of-plane tensile strain due to d_{33} coupling and in-plane compressive strain due to d_{31} coupling. Since the separation between the edges of each pair of electrodes (0.75 mm) is comparable to the substrate thickness, the interaction between the local strain fields generates biaxial strain in the piezoelectric substrate in the region where the nanomagnets are placed.[28] The resultant strain is tensile along the line joining AA′ and compressive along the direction perpendicular to it (see Figure S1 in the Supporting Information). It will be almost entirely transferred to the nanomagnets since the nanomagnets' thickness is much smaller than that of the substrate. A full strain profile was generated with finite element (FE) analysis and conformed to the above description (see Figure S1 in the Supporting Information).

Following the application of the voltage at electrode pair AA′, the same voltage (300 V) is applied to the electrode pair BB′, and subsequently AA′ is deactivated. Finally, the pair BB′ is also deactivated. Figure 2c shows the poststress MFM image. The magnetizations of the two nanomagnets in the top row have not changed under stress. One of them (at left) is stuck in the pinned state that even a 0.2 T magnetic field could not unpin. The other (at right) could also have been pinned or did not rotate through 180° owing to insufficient strain transfer. However, the remaining two nanomagnets in the bottom row have flipped their magnetizations (180° rotation) after the application of stress. In the Supporting Information, we discuss why and how some nanomagnets could experience insufficient strain. We can discount the top left nanomagnet whose magnetization is strongly pinned, in which case two out of three nanomagnets underwent complete magnetization reversal.

To examine any possible size dependence of this effect, we experimented with another set of nanomagnets (294 nm major axis, 272 nm minor axis, and thickness 8 nm) with the same center-to-center separation of 700 nm between nearest neighbors. These dimensions produce an in-plane shape

DOI: 10.1021/acs.nanolett.7b00439
Nano Lett. 2017, 17, 3478−3484

anisotropy energy barrier of 6.776 eV. Figure 3a shows the AFM image of six nominally identical nanomagnets. MFM

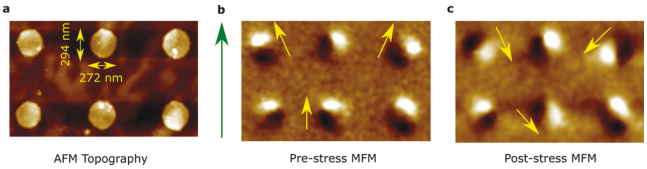

Figure 3. AFM and MFM images of six nominally identical larger elliptical Co nanomagnets delineated on a PMN−PT substrate showing how their magnetizations evolve with stress. (a) AFM image showing the topography of the six nanomagnets. (b) MFM image showing the magnetization states of the nanomagnets after magnetizing them with a ∼0.2 T magnetic field along the direction of the green arrow and before subjecting them to stress. (c) MFM image of the nanomagnets after subjecting them to sequential stress along two directions by sequentially activating the electrode pairs. The magnetizations of the two peripheral nanomagnets in the top row have rotated by 180° from their initial orientations (marked with yellow arrows). The nanomagnet in the middle of the bottom row has rotated by less than 180° and possibly got trapped into a metastable state. The other three nanomagnets are unresponsive to stress, either because the stress generated in them was insufficient to change their states (see Supporting Information for how and why this can happen) or their magnetizations have been pinned by spurious states.

images before and after the application of stress are shown in Figure 3b and c, respectively. After initialization with a magnetic field (in the direction of the green arrow along the major axes of the nanomagnets), the magnetizations of none of the six nanomagnets became exactly collinear with the major axes (or magnetic field) as shown in Figure 3b since, once again, the easy axes did not coincide with the major axes. The poststress MFM images (see Figure 3c) reveal that three out of the six nanomagnets (marked by the yellow arrows) have evolved to new magnetic states after experiencing the sequential stress cycle. The angular separation between the initial and final magnetic states is ∼180° for two out of these three, but one outlier has rotated by less than 180°, probably owing to trapping into an intervening metastable state that prevented complete magnetization reversal. In any case, there is no substantive difference with the previous set, meaning that both large and small nanomagnets behave in essentially the same way.

To show that the magnetization of a nanomagnet can be switched *back and forth* between two stable states with consecutive sequential stress cycles, we chose two sets of nanomagnets of thickness 8 nm: Set A with 294 nm major axis and 272 nm minor axis (Figure 4a), and Set B with 187 nm major axis and 164 nm minor axis (Figure 4c). The smaller set has an in-plane shape anisotropy energy barrier of 6.282 eV. Figure 4b illustrates the switching behavior of Set A nanomagnets in two successive sequential stress cycles. The prestress image shows the initial states of four nearest neighbor nanomagnets after magnetization with a magnetic field directed vertically up in this image. After completion of stress cycle 1 (AA′ and BB′ sequentially activated *once*), the top left nanomagnet (marked by yellow arrow) has rotated through 180° while the bottom right nanomagnet has evolved into a metastable state whose magnetization has a large angular deviation (almost 90°) from the major axis. The other two nanomagnets are unresponsive to stress (no difference between prestress and poststress). After cycle 2 (AA′ and BB′

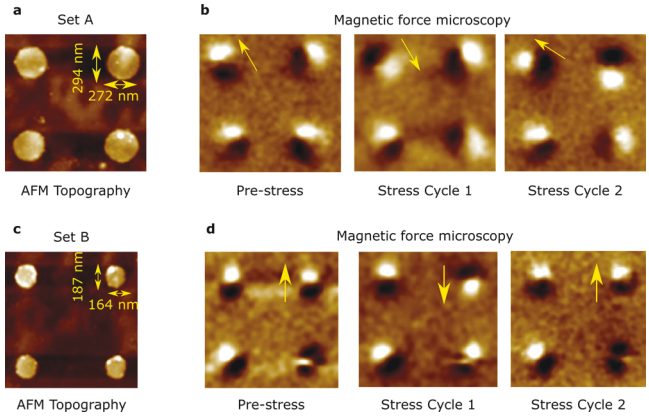

Figure 4. AFM and MFM images of two sets of Co nanomagnets (Set A and Set B) delineated on a PMN−PT substrate showing how their magnetizations react to two consecutive cycles of stress. Set A: four nanomagnets with major axis 294 nm and minor axis 272 nm. Set B: four nanomagnets with major axis 187 nm and minor axis 164 nm. (a, c) AFM image showing the topography of the four isolated nanomagnets. (b, d) The left panels show the MFM images of the initial states; the center panels show the MFM image after one sequential stress cycle indicating that the nanomagnets (marked by yellow arrows in b and d) experienced complete 180° rotation; the right panels show that the same nanomagnets marked with yellow arrows have undergone another ∼180° rotation and hence returned to their initial orientation after the second sequential stress cycle.

sequentially activated again), the same top left nanomagnet has rotated by about 160° and returned nearly to the original state, while the unresponsive nanomagnets have remained unresponsive and the one trapped into a metastable state has remained trapped there. Smaller nanomagnets (Set B) behave in the same way, as shown in Figure 4d, thereby demonstrating size-independence of the magnetization reversal scheme. In this set, the responsive nanomagnet undergoes ∼180° rotation in each cycle.

In Figure 5, we show the stress-induced magnetization changes in four sets of nanomagnets of four different sizes and ellipticity in the four rows. They all have different in-plane shape anisotropy energy barriers, but the generated stress should be able to overcome them in the manner of Figure 1b, and yet the MFM tip should not be able to alter the magnetization. This experiment was carried out to demonstrate that successive activation of *both* electrode pairs is required for magnetization reversal and that activation of only one pair will *not* bring about the 180° rotation. In each row, focus only on the nanomagnet that is marked with a yellow arrow since the other nanomagnets were unresponsive to stress. In the second column, we show the magnetization states of the nanomagnets after magnetization with a 0.2 T global magnetic field in the vertically up direction. In the third column, we show the magnetization states after activating and then deactivating only one pair of electrodes (e.g., AA′) and not the other. In the fourth column, we show the magnetization states after sequentially activating and then deactivating both pairs AA′ and BB′. Clearly, activating and deactivating only one pair does not change the state of the nanomagnets in any of the four cases shown (since the second and third columns are always identical). However, activating and deactivating both pairs in succession reverses the magnetization of the responsive nanomagnets in all four cases examined.

DOI: 10.1021/acs.nanolett.7b00439
Nano Lett. 2017, 17, 3478−3484

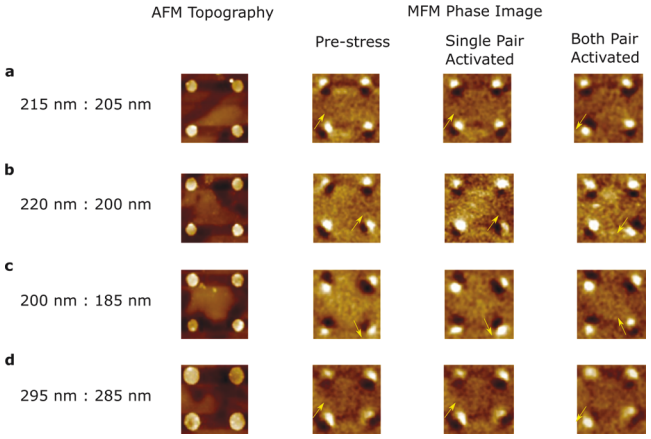

Figure 5. AFM and MFM micrographs of four sets of nanomagnets of different sizes and ellipticity showing how their magnetizations evolve when one and both pairs of electrodes are activated. The nominal dimensions (major and minor axes) are shown on the left in each horizontal panel. The calculated in-plane shape anisotropy energy barriers in these four sets are, respectively, 2.84 eV, 5.728 eV, 4.202 and 3.099 eV. The first column shows the topography of the four sets of nanomagnets, the second shows the initial magnetization states after magnetizing with a global magnetic field directed vertically up in this figure, the third shows the magnetization states after one pair of metal pads (say, AA′) is activated and then deactivated, while the fourth shows the magnetization states after both pairs are activated successively and deactivated successively.

What makes this magnetic reversal scheme attractive is the extremely low energy dissipated in the process. The dissipation has three components: the internal dissipation in the nanomagnets which is on the order of 1 aJ at room temperature,[32] the mechanical energy dissipation (stress × strain × volume of the nanomagnet) which is also a few aJ, and the electrical energy dissipated in the external circuit to activate the electrodes and generate stress in a nanomagnet. The last component is overwhelmingly dominant and is equal to CV^2, where C is the capacitance of the gate pairs and V is the voltage needed to generate the stresses. Let us now estimate how much energy would have been dissipated in a *properly scaled structure* where the separation between a single pair of electrodes is 100 nm, a single nanomagnet of lateral dimension ∼50 nm is placed between them, the electrode dimensions are of the same order (100 nm × 100 nm), and the PMN−PT film thickness is 100 nm. Since we applied 300 V across a 0.5 mm piezoelectric substrate to reverse magnetization, we will need to apply only 60 mV across a 100 nm thin film of piezoelectric to see the same effect (i.e., complete 180° rotation). The capacitance of one pair of electrodes will be $C = \epsilon_r\epsilon_0 A/d = 2 \times 500\times 8.854\times 10^{-12}$ F/m × 100 nm × 100 nm/100 nm = 0.88 fF, assuming a parallel plate capacitor (A is the area of the electrode, d is the piezoelectric film thickness and ϵ_r is the relative dielectric constant of the piezoelectric which is ∼500[41]). The energy dissipated to activate one pair is thus $CV^2 = 2 \times 0.88$ fF × $(60$ mV$)^2$ = 6.3 aJ and to activate both pairs is 13 aJ. This energy would be reduced further if we replace Co with a more magnetostrictive material like Terfenol-D or FeGa. Therefore, the energy dissipated to write one bit of information in a properly scaled memory cell will be a few tens of aJ at worst, which makes this one of the most energy-efficient writing schemes extant. The present experiment establishes a clear pathway to implementing such as scheme and portends an extremely energy-efficient MRAM technology.

One area of concern in these experiments is that the yield was poor (a small fraction of the nanomagnets switched while others were unresponsive to stress), but this can be improved substantially by choosing magnetostrictive materials that have much higher magnetostriction than Co (e.g., Terfenol-D, FeGa) (see Supporting Information) and by eliminating pinning sites with careful material preparation.

In conclusion, we have shown complete magnetization reversal in a magnetostrictive elliptical nanomagnet (with bistable magnetization) using mechanical strain generated by sequential electrode activation on a piezoelectric substrate. This can be utilized to write bits in nonvolatile memory cells with extremely low energy dissipation. The writing electrodes (four of them) are separate from the reading electrodes (two of them) which has its own advantage but also the disadvantage of a larger cell footprint which reduces the density of memory cells and calls for a more complex architecture. Thus, this scheme is attractive for low-energy, but not high-density, applications. There are many applications in mobile electronics, wearable electronics, space-based computers, and medically implanted processors where energy-efficiency outweighs all other considerations and this methodology of writing information in nonvolatile memory will be extremely attractive for those applications.

Methods. The fabrication process begins by poling a (011)-oriented $Pb(Mg_{1/3}Nb_{2/3})O_3$−$PbTiO_3$ (PMN−PT) (10 mm × 10 mm × 0.5 mm) substrate (70% PMN and 30% PT) with an electric field of 0.8 MV/m along the thickness by applying a positive voltage of 400 V on the top polished surface while grounding the bottom surface. Next, two pairs of large area metal pads Ti + Au (10 + 70 nm thickness) with lateral dimensions 0.4 mm × 0.4 mm are patterned on the surface of the substrate using photolithography and metal evaporation with e-beam, followed by lift-off. The lines joining the centers of opposite pairs subtend an angle of ∼60° between them. The distance between the facing edges of the electrodes in each pair is 0.75 mm, comparable to the thickness of the substrate. Next, elliptical Co nanomagnets are fabricated in the space between the electrodes with e-beam lithography (using multilayer PMMA), Co evaporation, and lift-off and aligned such that the major axes of all the nanomagnets subtend angles of approximately +30° and −30° with the two lines joining the centers of the two electrode pairs. The major axis is also aligned along the [100] crystal direction of the PMN−PT substrate. To carry out the e-beam lithography, two layers of e-beam resist PMMA [poly(methyl methacrylate)] with different molecular weights (495 and 950 K PMMA; 4% anisole) were spin-coated at 2500 rpm in two steps. The resists were baked at 115 °C for 2 min in each step. The sample was then exposed under electron beam from a Hitachi SU-70 SEM with a Nabity attachment using an accelerating voltage of 30 kV and a beam current of 60 pA. Subsequently, the resists were developed in MIBK:IPA (1:3) [(methyl isobutyl ketone−isopropyl alcohol)] solution for 90 s followed by cold IPA rinse. A Co layer of thickness of ∼8 nm is then deposited on the patterned resist using electron beam evaporation at a base pressure of 2×10^{-7} Torr with a Ti adhesion layer (thickness of 4 nm). A lift-off process was conducted for removing the resist and metal to produce the final nanomagnet pattern. Finally, the magnets are initialized by magnetizing them at room temperature with a

DOI: 10.1021/acs.nanolett.7b00439
Nano Lett. 2017, 17, 3478−3484

magnetic field of 0.2 T directed along the major axes of the ellipses, using an electromagnet.

■ ASSOCIATED CONTENT

Supporting Information

The Supporting Information is available free of charge on the ACS Publications website at DOI: 10.1021/acs.nanolett.7b00439.

Calculated strain profile underneath the nanomagnets using finite element methods (COMSOL Multiphysics package), micromagnetic simulations to support the magnetization dynamics, stress calculations to explain the failure of some nanomagnets to switch, calculations of the shape anisotropy energy barrier to show that stress anisotropy energy can overcome it, calculation of magnetization states at various stages of the stress cycle, the role of Gilbert damping, and discussions of various mechanisms of switching failure (PDF)

■ AUTHOR INFORMATION

Corresponding Author

*E-mail: sbandy@vcu.edu.

ORCID

Supriyo Bandyopadhyay: 0000-0001-6074-1212

Author Contributions

A.K.B. and H.A. contributed equally to the experimental work. All authors analyzed the data and contributed to writing the paper.

Notes

The authors declare no competing financial interest.

■ ACKNOWLEDGMENTS

This work is supported by the US National Science Foundation (NSF) under grants ECCS-1124714 and ECCS-1609303 and by the Semiconductor Research Corporation (SRC) under NRI task 2203.001. Additional funding was received from the State of Virginia Commonwealth Research Commercialization Fund under the matching fund grant MF-15-006-MS. J.A.'s work is also supported by NSF CAREER grant CCF-1253370.

■ REFERENCES

(1) Slonczewski, J. C. *J. Magn. Magn. Mater.* **1996**, *159*, L1−L7.
(2) Berger, L. *Phys. Rev. B: Condens. Matter Mater. Phys.* **1996**, *54*, 9353−9358.
(3) Sankey, J. C.; Cui, Y.-T.; Sun, J. Z.; Slonczewski, J. C.; Buhrman, R. A.; Ralph, D. C. *Nat. Phys.* **2008**, *4*, 67−71.
(4) Liu, L.; Pai, C.-F.; Li, Y.; Tseng, H. W.; Ralph, D. C.; Buhrman, R. A. *Science* **2012**, *336*, 555−558.
(5) Bhowmik, D.; You, L.; Salahuddin, S. *Nat. Nanotechnol.* **2013**, *9*, 59−63.
(6) Mellnik, A. R.; Lee, J. S.; Richardella, A.; Grab, J. L.; Mintun, P. J.; Fischer, M. H.; Vaezi, A.; Manchon, A.; Kim, E.-A.; Samarth, N.; Ralph, D. C. *Nature* **2014**, *511*, 449−451.
(7) Miron, I. M.; Garello, K.; Gaudin, G.; Zermatten, P.-J.; Costache, M. V.; Auffret, S.; Bandiera, S.; Rodmacq, B.; Schuhl, A.; Gambardella, P. *Nat. Mater.* **2011**, *10*, 419−423.
(8) Yu, G.; Upadhyaya, P.; Fan, Y.; Alzate, J. G.; Jiang, W.; Wong, K. L.; Takei, S.; Bender, S. A.; Chang, L.-T.; Jiang, Y.; Lang, M.; Tang, J.; Wang, Y.; Tserkovnyak, Y.; Amiri, P. K.; Wang, K. L. *Nat. Nanotechnol.* **2014**, *9*, 548−554.
(9) Fan, Y.; Upadhyaya, P.; Kou, X.; Lang, M.; Takei, S.; Wang, Z.; Tang, J.; He, L.; Chang, L.-T.; Montazeri, M.; Yu, G.; Jiang, W.; Nie, T.; Schwartz, R. N.; Tserkovnyak, Y.; Wang, K. L. *Nat. Mater.* **2014**, *13*, 699−704.
(10) Fan, Y.; Kou, X.; Upadhyaya, P.; Shao, Q.; Pan, L.; Lang, M.; Che, X.; Tang, J.; Montazeri, M.; Murata, K.; Chang, L.-T.; Akyol, M.; Yu, G.; Nie, T.; Wong, K. L.; Liu, J.; Wang, Y.; Tserkovnyak, Y.; Wang, K. L. *Nat. Nanotechnol.* **2016**, *11*, 352−359.
(11) Xiong, G.; Faulkner, C. C.; Atkinson, D.; Petit, D.; Cowburn, R. P. *Science* **2005**, *309*, 1688−1692.
(12) Yamanouchi, M.; Chiba, D.; Matsukura, F.; Ohno, H. *Nature* **2004**, *428*, 539−542.
(13) Wang, W.-G.; Li, M.; Hageman, S.; Chien, C. L. *Nat. Mater.* **2011**, *11*, 64−68.
(14) Chu, Y.-H.; Martin, L. W.; Holcomb, M. B.; Gajek, M.; Han, S.-J.; He, Q.; Balke, N.; Yang, D.; Lee, C.-H.; Hu, W.; Zhan, Q.; Yang, P.-L.; Fraile-Rodriguez, A.; Scholl, A.; Wang, A.; Ramesh, R. *Nat. Mater.* **2008**, *7*, 478−482.
(15) Heron, J. T.; Bosse, J. L.; He, Q.; Gao, Y.; Trassin, M.; Ye, L.; Clarkson, J. D.; Wang, C.; Liu, J.; Salahuddin, S.; Ralph, D. C.; Schlom, D. G.; Iniguez, J.; Huey, B. D.; Ramesh, R. *Nature* **2014**, *516*, 370−373.
(16) Matsukura, F.; Tokura, Y.; Ohno, H. *Nat. Nanotechnol.* **2015**, *10*, 209−220.
(17) Bauer, U.; Yao, L.; Tan, A. J.; Agrawal, P.; Emori, S.; Tuller, H. L.; van Dijken, S.; Beach, G. S. D. *Nat. Mater.* **2014**, *14*, 174−181.
(18) Novosad, V.; Otani, Y.; Ohsawa, A.; Kim, S. G.; Fukamichi, K.; Koike, J.; Maruyama, K.; Kitakami, O.; Shimada, Y. *J. Appl. Phys.* **2000**, *87*, 6400−6402.
(19) Eerenstein, W.; Mathur, N. D.; Scott, J. F. *Nature* **2006**, *442*, 759−765.
(20) Pertsev, N. A.; Kohlstedt, H. *Appl. Phys. Lett.* **2009**, *95*, 163503.
(21) Atulasimha, J.; Bandyopadhyay, S. *Appl. Phys. Lett.* **2010**, *97*, 173105.
(22) Wu, T.; Bur, A.; Wong, K.; Zhao, P.; Lynch, C. S.; Amiri, P. K.; Wang, K. L.; Carman, G. P. *Appl. Phys. Lett.* **2011**, *98*, 262504.
(23) Giordano, S.; Dusch, Y.; Tiercelin, N.; Pernod, P.; Preobrazhensky, V. *Phys. Rev. B: Condens. Matter Mater. Phys.* **2012**, *85*, 155321.
(24) Biswas, A. K.; Bandyopadhyay, S.; Atulasimha, J. *Appl. Phys. Lett.* **2014**, *104*, 232403.
(25) Li, P.; Chen, A.; Li, D.; Zhao, Y.; Zhang, S.; Yang, L.; Liu, Y.; Zhu, M.; Zhang, H.; Han, X. *Adv. Mater.* **2014**, *26*, 4320−4325.
(26) Fukami, S.; Suzuki, T.; Nagahara, K.; Ohshima, N.; Ozaki, Y.; Saito, S.; Nebashi, R.; Sakimura, N.; Honjo, H.; Mori, K.; Igarashi, C.; Miura, S.; Ishiwata, N.; Sugibayashi, T. *2009 IEEE Symp. VLSI Technol. Dig. Technol. Pap.* **2009**, 230−231.
(27) Amiri, P. K.; Wang, K. L. *SPIN* **2012**, *2*, 1240002.
(28) Cui, J.; Hockel, J. L.; Nordeen, P. K.; Pisani, D. M.; Liang, C.-y.; Carman, G. P.; Lynch, C. S. *Appl. Phys. Lett.* **2013**, *103*, 232905.
(29) Liang, C.-Y.; Keller, S. M.; Sepulveda, A. E.; Sun, W.-Y.; Cui, J.; Lynch, C. S.; Carman, G. P. *J. Appl. Phys.* **2014**, *116*, 123909.
(30) Cui, J.; Liang, C.-Y.; Paisley, E. A.; Sepulveda, A.; Ihlefeld, J. F.; Carman, G. P.; Lynch, C. S. *Appl. Phys. Lett.* **2015**, *107*, 092903.
(31) Roy, K.; Bandyopadhyay, S.; Atulasimha, J. *Appl. Phys. Lett.* **2011**, *99*, 063108.
(32) Roy, K.; Bandyopadhyay, S.; Atulasimha, J. *J. Appl. Phys.* **2012**, *112*, 023914.
(33) Fashami, M. S.; Roy, K.; Atulasimha, J.; Bandyopadhyay, S. *Nanotechnology* **2011**, *22*, 155201.
(34) Ahmad, H.; Atulasimha, J.; Bandyopadhyay, S. *Sci. Rep.* **2016**, *5*, 18264.
(35) D'Souza, N.; Salehi Fashami, M.; Bandyopadhyay, S.; Atulasimha, J. *Nano Lett.* **2016**, *16*, 1069−1075.
(36) Zhao, Z.; Jamali, M.; D'Souza, N.; Zhang, D.; Bandyopadhyay, S.; Atulasimha, J.; Wang, J.-P. *Appl. Phys. Lett.* **2016**, *109*, 092403.
(37) Biswas, A. K.; Bandyopadhyay, S.; Atulasimha, J. *Appl. Phys. Lett.* **2014**, *105*, 072408.
(38) Roy, K.; Bandyopadhyay, S.; Atulasimha, J. *Sci. Rep.* **2013**, *3*, 3038.

DOI: 10.1021/acs.nanolett.7b00439
Nano Lett. 2017, 17, 3478−3484

(39) Peng, R.-C.; Hu, J.-M.; Momeni, K.; Wang, J.-J.; Chen, L.-Q.; Nan, C.-W. *Sci. Rep.* **2016**, *6*, 27561.
(40) Wang, J.-J.; Hu, J.-M.; Ma, J.; Zhang, J. X.; Chen, L.-Q.; Nan, C.-W. *Sci. Rep.* **2015**, *4*, 7507.
(41) Shaikh, P. A.; Kolekar, Y. D. *J. Anal. Appl. Pyrolysis* **2012**, *93*, 41−46.

DOI: 10.1021/acs.nanolett.7b00439
Nano Lett. 2017, 17, 3478−3484